

Joint time-variant spectral analysis — Part 1: Forward modeling the effects of thin-bed layering

Ramses G. Meza¹, J. Antonio Sierra², John P. Castagna³, and Umberto Barbato⁴

Abstract

Using time-frequency and time-phase analysis we found that for an isolated thin bed in a binary-impedance setting, there is no observable sensitivity in preferential illumination as layered net-to-gross (NTG) changes within the isolated thin bed, regardless of the way the internal layering is distributed — either uniformly or semirandomly. The NTG signature is observed on the amplitude (magnitude) responses, rather than any specific frequency or phase component. On the other hand, external mutual thin-bed interference can significantly change the preferred phase component for each participating target. This phenomenon is largely driven by the embedded seismic wavelet that determines the nominal seismic response of an isolated thin layer and what phase component would preferentially illuminate it. For vertical separations between mutually interfering and elastically comparable thin beds in which mutual constructive interference is achieved, the target bed will be preferentially illuminated at a phase component that is very close to that of a total seismic isolation, whereas the occurrence of mutual destructive interference will cause a significant departure on the phase preferential illumination from that of an isolated seismic thin bed. All these observations can provide an avenue to yield more robust stratigraphic interpretations of seismic data and enhance the confidence on subsurface description.

Introduction

Quantitative interpretation (QI) of reflection seismic data has the objective of estimating subsurface rock properties and/or environmental conditions that can explain the geophysical observations within a given geologic framework. This means that the adoption of any subsurface scenario as a valid interpretation of the geophysical observations must be supported by a robust model that simulates the observations within some acceptable degree of uncertainty.

In exploration geophysics for hydrocarbons, most QI-related research and development efforts have been directed toward the detection and/or characterization of lithology, pore-fluid content, and porosity, which have been assumed to be the first-order drivers of the seismic observations associated with layers of interest (Avseth et al., 2010; Chopra and Castagna, 2014; Simm and Bacon, 2014). Similar importance must be given to the underlying rock layering, which is the vertical stacking patterns of layers of different elastic properties. Such patterns can manifest as different bedding attributes, such as layer thickness, net-to-gross (NTG) ratio, and clustering. Here, we define NTG as the proportion of a depositional sequence or formation/member gross

rock thickness that corresponds to net thickness of a nonbackground lithology. For instance, in mud-dominated (background lithology) clastic depositional sequences, sandstones commonly represent the nonbackground lithology.

Brown et al. (1984, 1986) are among the first to recognize and empirically quantify the effect of NTG on seismic amplitudes for thin beds, using it as an avenue for estimation of net sand by means of detuning the seismic amplitudes, which implicitly depends on the underlying spectral characteristics of the seismic data. Connolly (2007) uses relative or band-limited inverted seismic data obtained via colored inversion as defined by Lancaster and Whitcombe (2000), who also observe a power-law behavior of the impedance spectra with a real-negative spectral scalar α . The reflectivity and impedance power-law behaviors can be taken as evidence of the statistically fractal nature of the stratigraphic record (Dolan et al., 1998; Bailey and Smith, 2005; Browaeys and Fomel, 2009). This implies that the stratigraphic record is scale invariant with layering characteristics that may be described by means of spectral analysis (Turcotte, 1997; Dimri, 2005).

The contributions of spectral constituents of any signal have been historically determined by means of the

¹BHP Billiton Petroleum, Mexico Regional Exploration, Houston, Texas, USA. E-mail: ramses.meza@bhp.com.

²EOG Resources, Houston, Texas, USA. E-mail: antonio_sierra@eogresources.com.

³University of Houston, Houston, Texas, USA. E-mail: jcastagnaou@yahoo.com.

⁴Lumina Geophysical, Houston, Texas, USA. E-mail: umberto.barbato@luminageo.com.

Manuscript received by the Editor 15 February 2018; revised manuscript received 17 May 2018; published ahead of production 11 July 2018. This paper appears in *Interpretation*, Vol. 6, No. 4 (November 2018); p. 1–17, 19 FIGS.

<http://dx.doi.org/10.1190/INT-2018-0048.1>. © 2018 Society of Exploration Geophysicists and American Association of Petroleum Geologists. All rights reserved.

Fourier transform (Bracewell, 2000). However, this poses limitations in cases in which there is a need to analyze the spectral behavior of a signal in a time-variant basis, especially where target single thin-bed seismic isolation is unlikely or absent. Time-frequency analysis or spectral decomposition (Chakraborty and Okaya, 1995; Okaya, 1995; Partyka et al., 1999; Castagna et al., 2003) has been developed as an interpretation tool with a focus on optimizing the temporal and frequency localization of events in which the localized spectra are used to draw inferences about a reflecting event, especially in cases of thin beds. Regardless of the spectral decomposition algorithm used to obtain time-variant spectra, only the magnitude component has been commonly used, whereas the time-variant phase spectrum has proven to be very difficult to interpret.

To overcome this subusage of time-variant spectral information, Castagna et al. (2016) develop a time-phase analysis technique called phase decomposition (PD), which is a time-variant expression of amplitudes as a function of the signal phase components within a frequency bandwidth. Meza et al. (2016) show some very interesting results of the technique in which different phase components are unmistakably highlighted depending on the target bed relative structural position or terrain. The ability to successfully use time-frequency and time-phase analysis relies on the concept of preferential illumination (Castagna et al., 2003). Seismic events are preferentially illuminated by certain frequency and phase components, which allows drawing inferences about the subsurface that may not be possible without decomposing the input seismic data set. Seismic resolution imposes a limit on our ability to directly interpret finer scale layering based on the identification of discrete reflections from individual stratigraphic interfaces. High-resolution modern postprocessing techniques such as spectral inversion (Puryear and Castagna, 2008) can greatly assist such an endeavor. However, this kind of technique requires a high signal-to-noise ratio (S/N) and precise control of the phase via several well-seismic ties. This may only be possible in the early to mature stages of hydrocarbon development, but not during exploration activities lacking well control, where the need to reduce the stratigraphic uncertainty is of the utmost importance.

This paper investigates the idea that layering can yield seismic signatures in the spectral domain, which can possibly be used to assist in improving the stratigraphic description of the subsurface. The effect of the NTG of a composite thin bed on joint frequency and time-PD is studied by means of forward-modeling examples to provide supporting evidence that certain layering characteristics, especially mutual thin-bed interference, might be inferred from such analysis. Our goal is to systematically deploy some spectral-based analysis criteria closer to the seismic interpreter, rather than the seismic specialist or analyst that can help in increasing the understanding of the stratigraphic record and help constraining the subsurface solution space. Achieving this would enhance

our confidence in the predictions of subsurface properties before any direct measurement is made.

Time-variant spectral analysis for modeled uniform layering

Time-frequency analysis (magnitude analysis of spectral decomposition)

High-resolution time-frequency analysis was performed using the constrained least-squares spectral analysis (CLSSA) (Puryear et al., 2012), which is a time-frequency analysis technique that yields time-variant spectra with the highest time and frequency resolution combination for all frequencies. For a single-trace vertical-sliding window of a given length (commonly 40 ms), CLSSA yields the spectra by using least-squares analysis to solve the Fourier series coefficients that characterize the seismic signal within the window. All the synthetic seismic signals analyzed on this paper were built convolving a Ricker wavelet of a specific central frequency with the reflectivity series yielded by the corresponding binary-acoustic impedance earth model (all shales having one constant impedance value, and all sands having another constant impedance value). The temporal sampling rate is 1 ms, and the frequency axis in all figures ranges from 0 to 125 Hz for ease of display of the preferential illumination.

Figure 1a–1c depicts some NTG scenarios in which synthetic seismic was generated (Figure 1d–1f), and CLSSA was applied to generate the corresponding magnitude components displayed as frequency gathers (Figure 1g–1i). Visual inspection of the frequency gather allows inferring that peak frequency (the frequency at which the spectral maximum or peak magnitude occurs) is nearly the same for the NTG scenarios shown, with a clear reduction of the peak magnitude as the NTG becomes lower. Figure 2 shows the actual dependence of the composite amplitude (the sum of the absolute amplitude values of the bed top and base reflections), peak magnitude (the maximum magnitude on the magnitude spectrum for a given two-way time), and peak frequency (the frequency on the magnitude spectrum at which the peak magnitude occurs) with all the synthetic NTG scenarios. As expected, composite amplitude varies almost linearly with NTG (Brown et al., 1984, 1986; Connolly, 2007). However, such semilinear dependence is less evident for peak magnitude. In the case of peak frequency, values for each NTG are very close to each other with no evident functional correlation with NTG. However, all peak frequencies are lower than that of the wavelet (25 Hz).

Time-phase analysis (PD)

Historically, time-variant spectral analysis has been largely focused on the analysis of the magnitude of spectral constituents of a signal, allowing us to characterize it based on how certain spectral components allow preferential illumination of the signal at a given traveltime. The time-variant phase spectrum is also an output of time-frequency analysis, but it has proven to

be extremely difficult to interpret in most cases. Castagna et al. (2016) develop a technique to better analyze the time-variant phase spectra, which is called phase

decomposition (PD). This technique yields amplitude values as a function of phase at a given travelttime within a frequency bandwidth. Similarly to CLSSA, PD

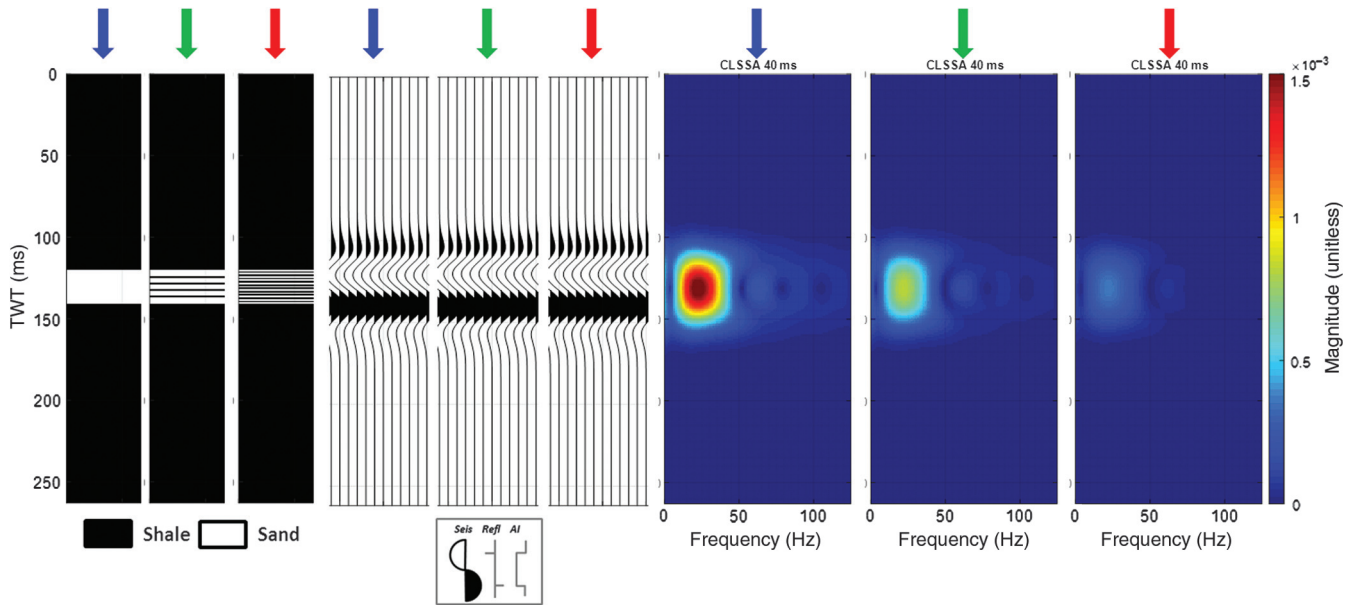


Figure 1. Bed facies model displaying interbedded layers of sand (white) and shale (black) within a 20 ms thick bed with (a) NTG = 100%, (b) 80.95%, and (c) 52.38%. Synthetic seismic response (the same trace repeated 11 times) using a 25 Hz zero-phase Ricker wavelet for (d) NTG= 100%, (e) 80.95%, and (f) 52.38%. The corresponding frequency gather based on a CLSSA 40 ms window time-frequency analysis of a single trace from the synthetic seismic responses for (g) NTG = 100%, (h) 80.95%, and (i) 52.38%. For ease of comparison, the bed facies model, synthetic seismic and frequency gather for NTG = 100% are indicated by a blue arrow, NTG = 80.95% are indicated by a green arrow, and NTG = 52.38% are indicated by a red arrow.

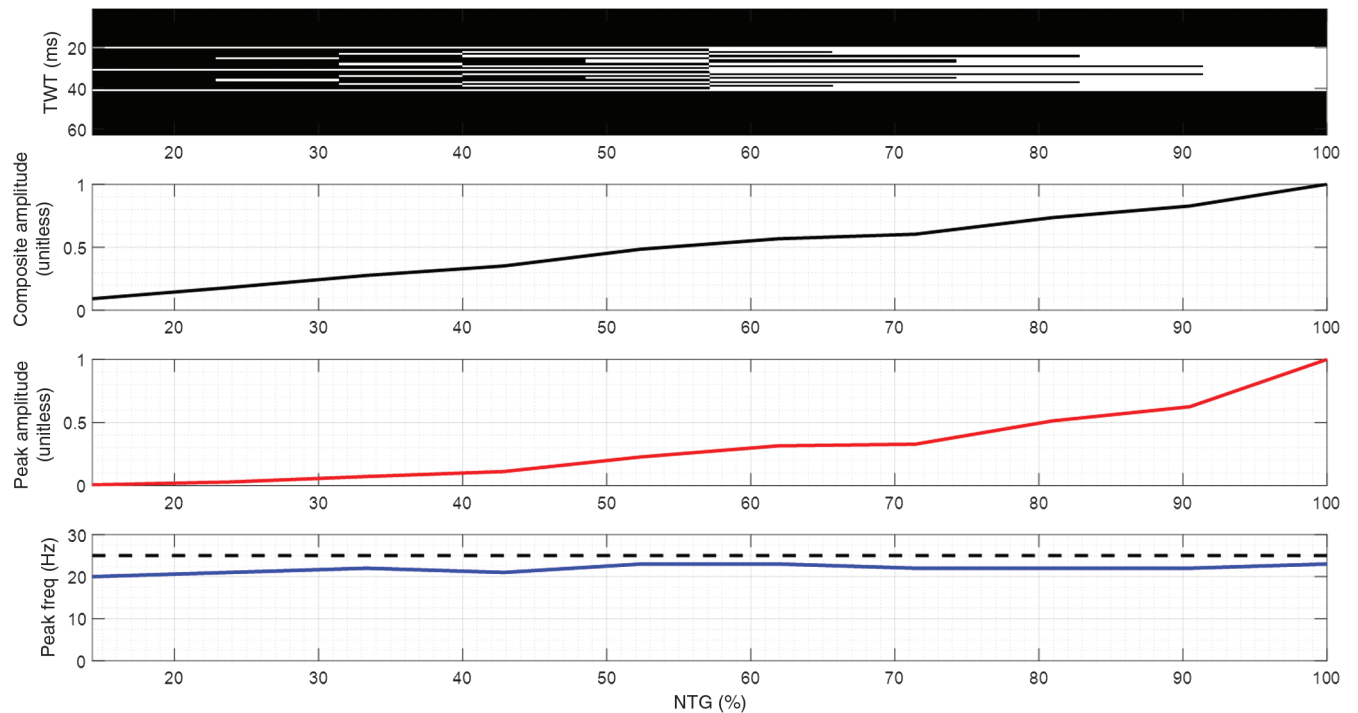


Figure 2. Comparison of attributes for a 20 ms thick bed for varying layered NTG (minimum NTG = 14.29%): (a) bed facies model displaying interbedded layers of sand (white) and shale (black), (b) composite amplitude (normalized), (c) peak magnitude (normalized) out of CLSSA time-frequency analysis, and (d) peak frequency out of CLSSA time-frequency analysis. The dashed line is the Ricker wavelet frequency.

was designed to be energy preserving, which means that the summation of amplitudes for all phase components will closely reproduce the input signal.

PD preferential illumination could also be understood by analyzing the synthetic response for three end-member reflectivity scenarios: First, for an isolated reflection coefficient (Figure 3a) convolved with a wavelet (Figure 3b), the phase gather yielded by the PD of the seismic trace (Figure 3c) will show preferential illumination at the phase of the wavelet — in this case, a zero-phase 25 Hz Ricker wavelet. Second, when considering the case of a thin bed such that its top and

base reflection coefficients — a dipole — have equal magnitude and polarity (Figure 3d), the resulting synthetic seismic trace (Figure 3e) will yield a phase gather (Figure 3f) that still shows the same preferential phase illumination as the wavelet. Finally, for the case of a thin bed such that it yields a dipole of reflection coefficients of equal magnitude and opposite polarity (Figure 3g), the resulting synthetic seismic trace (Figure 3h) will generate a phase gather (Figure 3i) that exhibits a preferential phase illumination at -90° with respect to the phase of the wavelet. A polarity reversal of the dipole in this case will cause a preferential phase illumination

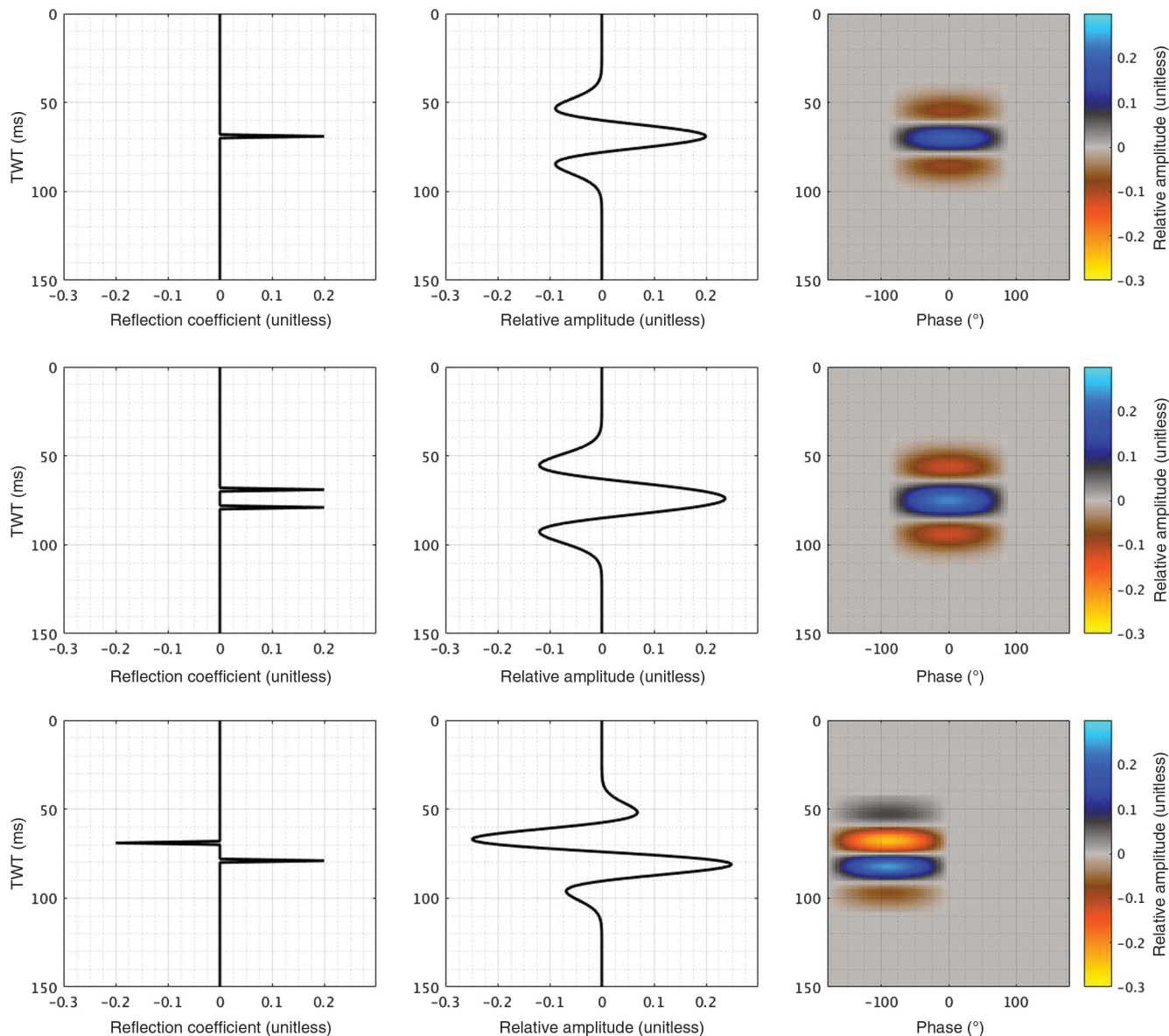


Figure 3. Example of PD on thin beds: (a) reflectivity series with a single reflection coefficient, (b) synthetic seismic as a result of the convolution of the reflectivity series (a) with a 25 Hz zero-phase Ricker wavelet, (c) phase gather yielded by the PD of the synthetic seismic on (b), (d) reflectivity series with two reflection coefficients of equal magnitude and sign, (e) synthetic seismic as a result of the convolution of the reflectivity series (d) with a 25 Hz zero-phase Ricker wavelet, (f) phase gather yielded by the PD of the synthetic seismic on (e), (g) reflectivity series with two reflection coefficients of equal magnitude and opposite sign, (h) synthetic seismic as a result of the convolution of the reflectivity series (g) with a 25 Hz zero-phase Ricker wavelet, and (i) phase gather yielded by the PD of the synthetic seismic on (h).

at $+90^\circ$ instead. From all these observations can also be inferred that, for a seismic thick bed with any kind of dipole reflectivity, the corresponding preferential phase illumination for each reflection will be either 0° or 180° with respect to the phase of the embedded wavelet, depending on the individual reflection polarity.

Figure 4a–4c shows the same earth models as used in Figure 1a–1c, which yielded the synthetic seismic responses that are shown in Figure 4d–4f. The corresponding phase gathers for these synthetic seismic responses are shown in Figure 4g–4i. Visual inspection of these phase gathers allows noting that preferential phase illumination is achieved approximately -90° , and amplitudes on phase gathers rise as the NTG rises. A more quantitative view of these observations is depicted in Figure 5, which considers all NTG scenarios modeled so far. In this context, PD peak amplitude is the absolute largest amplitude on each phase gather, whereas PD peak phase is the phase angle value at which PD peak amplitude is reached. Because for all NTG scenarios (except the lowest modeled NTG = 14.29%), the 20 ms thick bed yields the seismic response of a thin bed, then it comes as no surprise that the PD peak phase for each NTG scenario is -90° , which is the phase of a waveform corresponding to a lower impedance thin bed for a zero-phase seismic signal (Widess, 1973). Despite that there is waveform interference due to internal layering, it is not expressed as a variation of PD peak phase with NTG because each scenario was constructed in such a way that layering is symmetrical with respect to the center of the 20 ms thick layer. PD peak amplitude, on the other hand, shows an almost linear dependence

with NTG that resembles very much that of the composite amplitude.

Time-variant spectral analysis for modeled complex layering

Assuming that other first-order variables that influence seismic response are held constant, pursuing a time-variant spectral analysis to make inferences about layering features (such as NTG) for thin beds may become a marginal-return enterprise because conventional seismic amplitude analysis alone may assist with that purpose. However, the synthetic responses analyzed before are subject to the following design limitations:

- 1) Symmetric/uniform layering: NTG scenarios were built such that there is always vertical layering symmetry and elastic uniformity within the bed. For a thin bed with an effective impedance lower than that of the encasing media, PD is expected to always yield preferential phase illumination for the same phase angle — in this case -90° . Such symmetry is not commonly observed in actual depositional beds (Miall, 2010); therefore, under asymmetric vertical layering within a thin bed is reasonable to expect variations on the preferential phase illumination, even for constant NTG.
- 2) Constant gross thickness: This imposes a constraint to preferential frequency illumination as stated before because the same apparent gross-thickness beds will achieve preferential frequency illumination at nearly the same peak frequency.

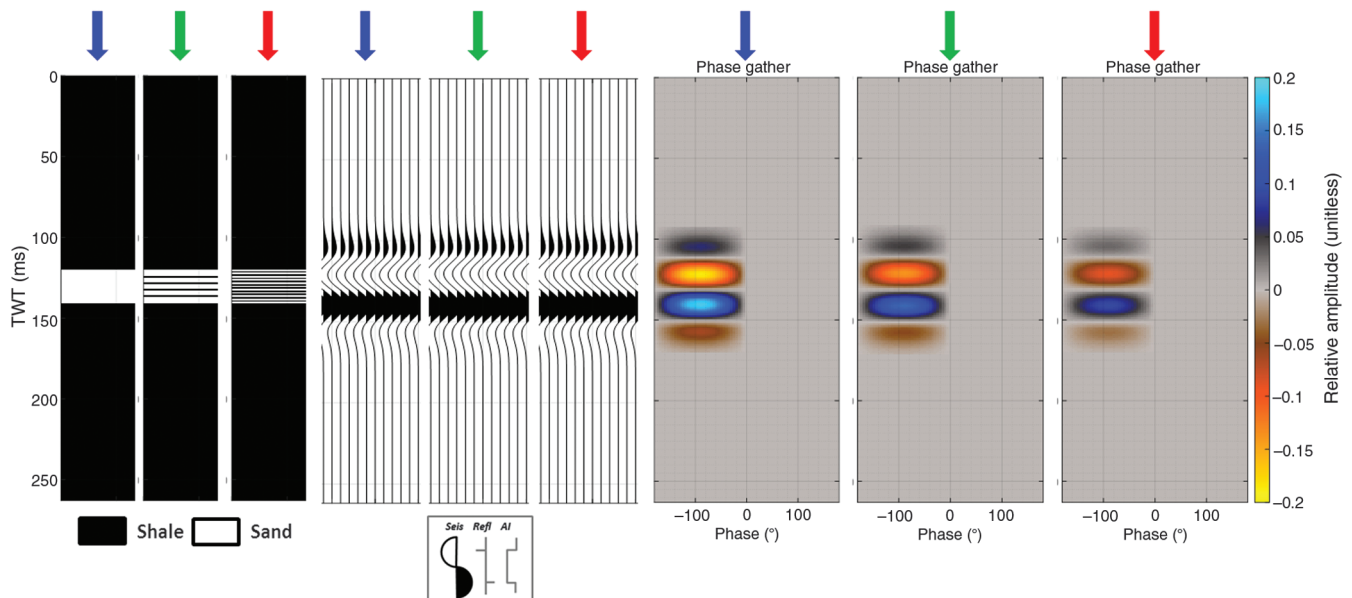


Figure 4. Bed facies model displaying interbedded layers of sand (white) and shale (black) within a 20 ms thick bed with (a) NTG = 100%, (b) 80.95%, and (c) 52.38%. Synthetic seismic response (same trace repeated 11 times) using a 25 Hz zero-phase Ricker wavelet for (d) NTG = 100%, (e) 80.95%, and (f) 52.38%. The corresponding phase gather yielded by the PD of a single trace from the synthetic seismic responses for (g) NTG = 100%, (h) 80.95%, and (i) 52.38%. For ease of comparison, the bed facies model, synthetic seismic and phase gather for NTG = 100% are indicated by a blue arrow, NTG = 80.95% are indicated by a green arrow, and NTG = 52.38% are indicated by a red arrow.

This imposes the need to perform forward modeling that yields asymmetric vertical layering and variations in apparent gross thickness, which produce enough scenarios to describe the effects of layering on the time-variant spectral analysis of a thin bed. These models can be generated by using pseudorandom mathematical processes, such as Markov chains, which have been reported to be able to yield discrete stratigraphic markers or lithology/facies flags that in many cases resemble those of actual depositional sequences (Davis, 2002; Dvorkin et al., 2014). Markov chain outcomes are controlled by an $n \times n$ matrix called the transition matrix P , where n is the number of mutually exclusive states (i.e., facies/lithologies), and each element p_{ij} on the transition matrix represents the conditional probability of transitioning from the i th state to the j th state at a given iteration or step. For the case of binary facies (i.e., shales and sands), the transition matrix takes the form

$$P = \begin{pmatrix} p_{11} & p_{12} \\ p_{21} & p_{22} \end{pmatrix}, \quad (1)$$

where $i, j = 1$ represents the shale and $i, j = 2$ represents the sand. Off-diagonal terms are the conditional probabilities of transition from shale to sand (p_{12}) or from sand to shale (p_{21}). Diagonal elements are the conditional probabilities of transition from shale to shale (p_{11}) or sand to sand (p_{22}). A large diagonal conditional probability will tend to yield thicker layers on the modeled stratal sequence for that particular lithology/facies, whereas large off-diagonal elements will tend to increase the alter-

nations or layering between the involved lithologies. Because all the conditional probabilities along any i th row on a transition matrix must add to one, the transition matrix P in equation 1 can be rewritten as a function of p_{11} and p_{22} only:

$$P = \begin{pmatrix} p_{11} & 1 - p_{11} \\ 1 - p_{22} & p_{22} \end{pmatrix}. \quad (2)$$

It is intuitive that sets of stratal sequences built using the same conditional probabilities and length/thickness may have different appearances, especially for shorter sequences. Hence, it can be expected that seismic responses can differ from one another for the same set of conditional probabilities. For the case of a 20 ms thick bed, Figures 6, 7, 8, and 9 show how the synthetic seismic and its time-frequency (CLSSA) and time-phase (PD) responses change as the layering distribution (controlled by p_{11} and p_{22}) within the bed changes. Figure 6 represents the base case in which the 20 ms thick target bed is 100% NTG, displaying vertically symmetric seismic response. The same symmetry can be observed on the frequency gather and the phase gather. By introducing layering variability within the target layer, as shown in Figures 7–9, it can be observed that amplitudes (seismic, CLSSA peak amplitude, and PD peak amplitude) are changing with layering/NTG although not linearly as with the case with uniformly distributed layering. CLSSA peak frequency and PD peak phase depict very small changes, if any. The PD peak phase is very close to -90° for all cases, which is what is expected for a lower impedance thin bed.

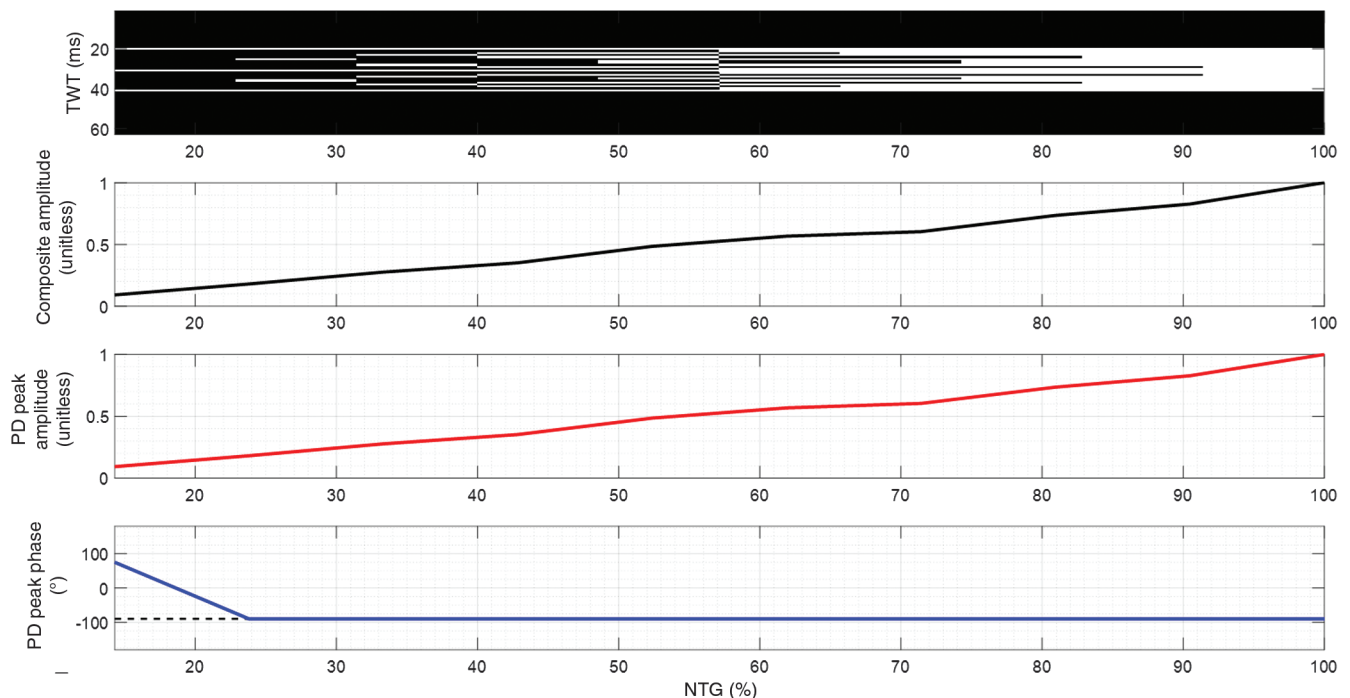


Figure 5. Comparison of attributes for a 20 ms thick bed for varying layered NTG (minimum NTG = 14.29%): (a) bed facies model displaying interbedded layers of sand (white) and shale (black), (b) composite amplitude (normalized), (c) PD peak amplitude (normalized) out of PD, and (d) PD peak phase out PD. The dashed line is -90° .

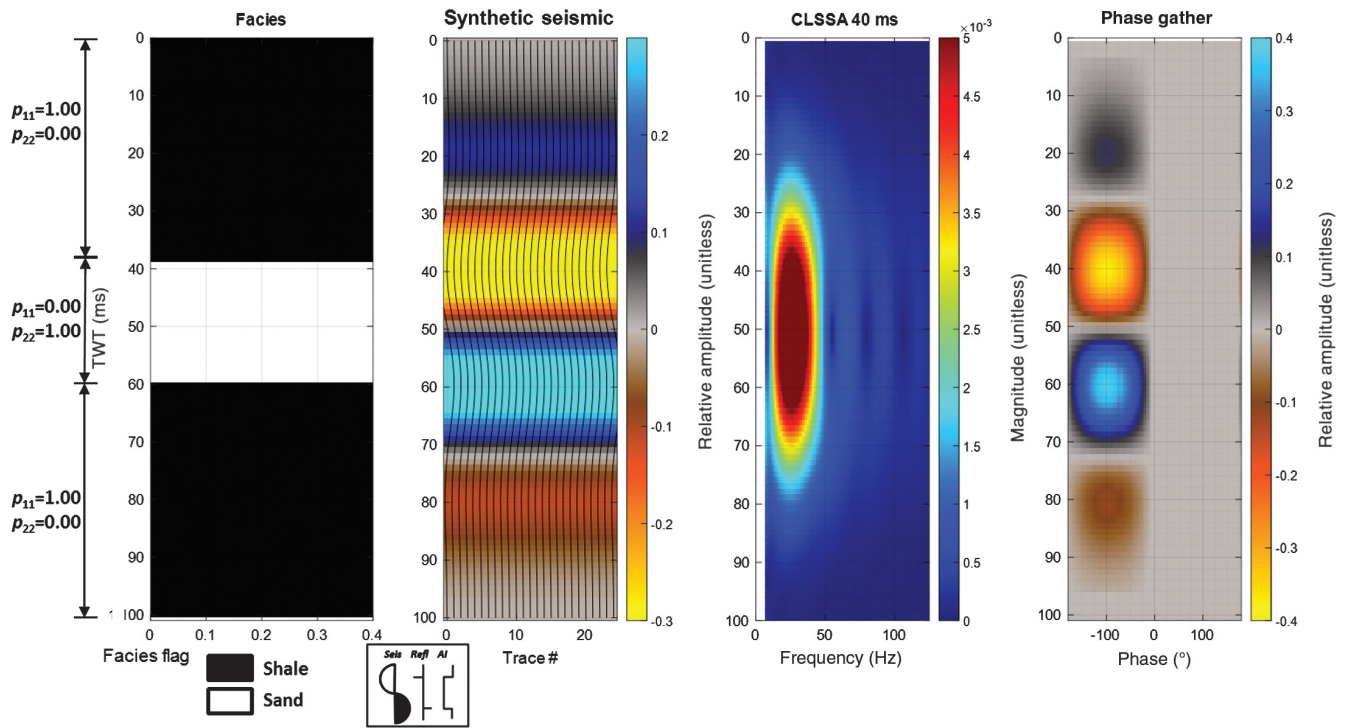


Figure 6. Simulation (base case) using the conditional probabilities indicated on the far left for a 20 ms long stratal binary sequence: (a) bed facies model displaying interbedded layers of sand (white) and shale (black), (b) synthetic seismic response (same trace repeated 25 times) using a 20 Hz zero-phase Ricker wavelet, (c) frequency gather based on a CLSSA 40 ms window time-frequency analysis of a single trace from the synthetic seismic, and (d) phase gather yielded by the PD of a single trace from the synthetic seismic response.

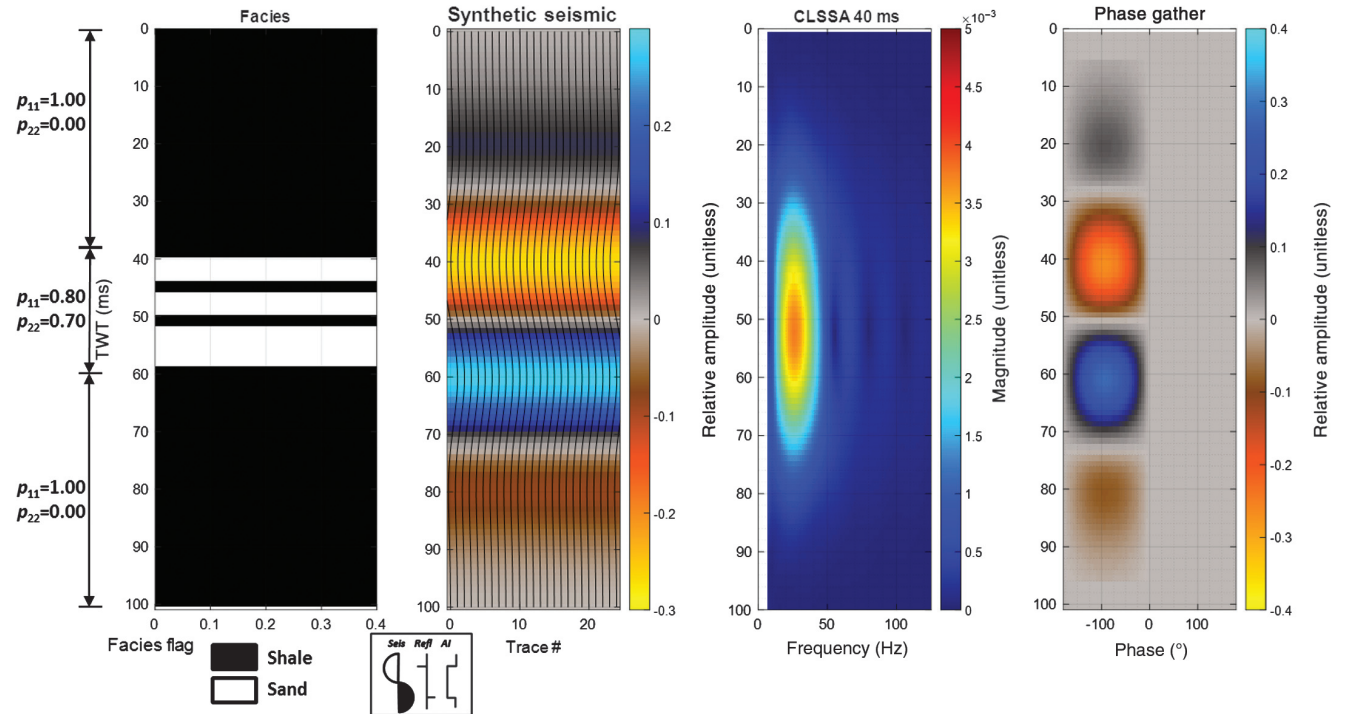


Figure 7. Simulation 1 using the conditional probabilities indicated on the far left for a 20 ms long stratal binary sequence: (a) bed facies model displaying interbedded layers of sand (white) and shale (black), (b) synthetic seismic response (same trace repeated 25 times) using a 20 Hz zero-phase Ricker wavelet, (c) frequency gather based on a CLSSA 40 ms window time-frequency analysis of a single trace from the synthetic seismic, and (d) phase gather yielded by the PD of a single trace from the synthetic seismic response.

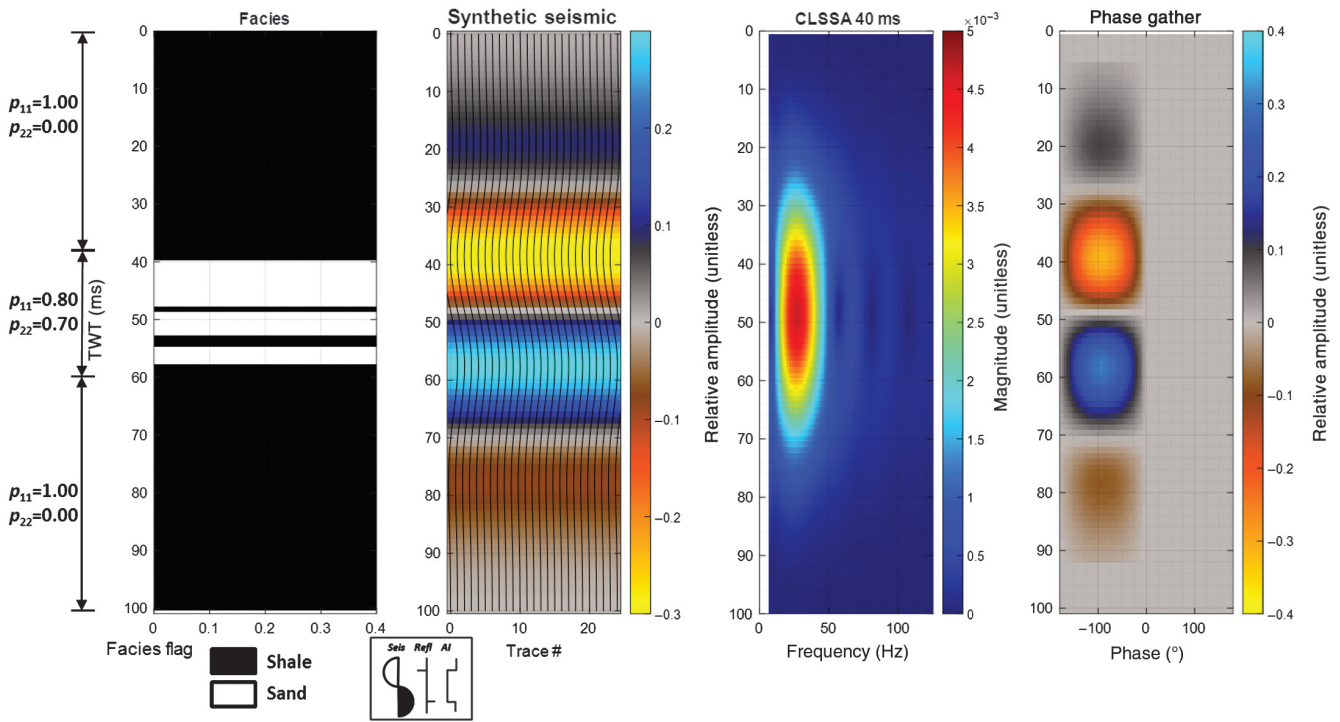


Figure 8. Simulation 2 using the conditional probabilities indicated on the far left for a 20 ms long stratal binary sequence: (a) bed facies model displaying interbedded layers of sand (white) and shale (black), (b) synthetic seismic response (same trace repeated 25 times) using a 20 Hz zero-phase Ricker wavelet, (c) frequency gather based on a CLSSA 40 ms window time-frequency analysis of a single trace from the synthetic seismic, and (d) phase gather yielded by the PD of a single trace from the synthetic seismic response.

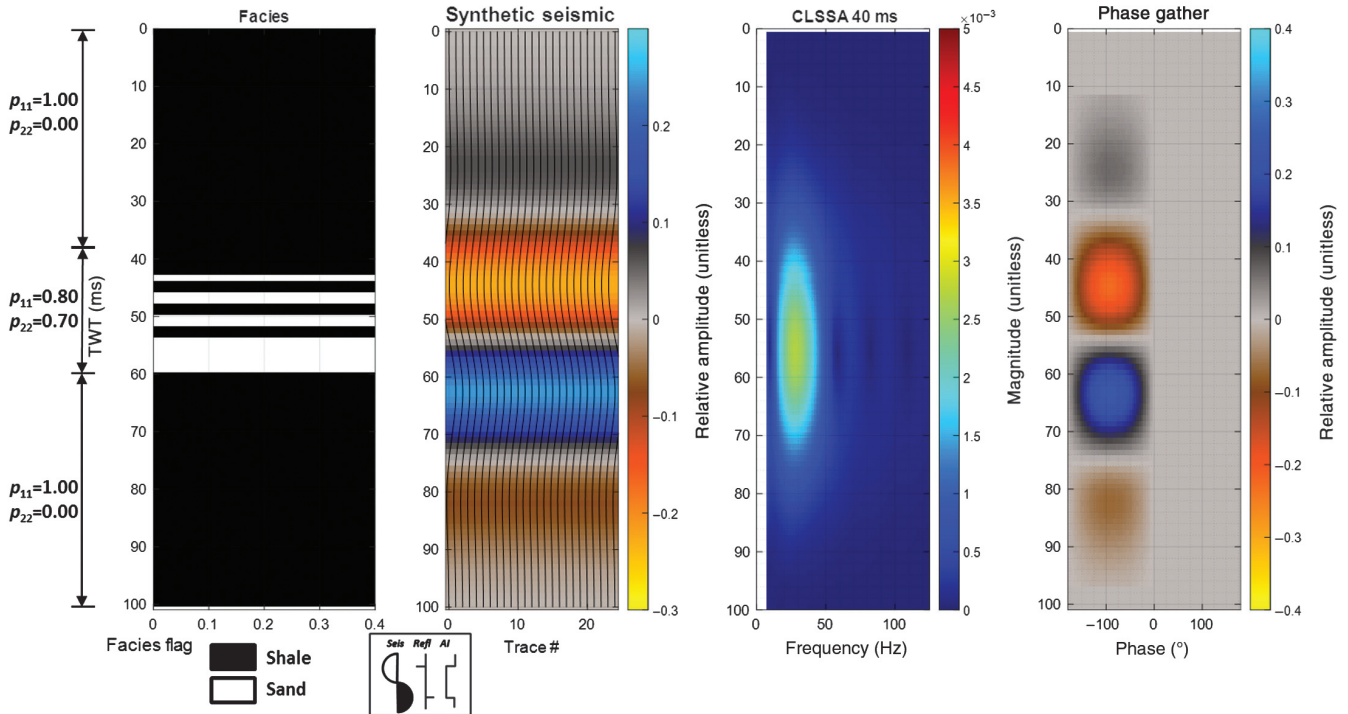


Figure 9. Simulation 3 using the conditional probabilities indicated on the far left for a 20 ms long stratal binary sequence: (a) bed facies model displaying interbedded layers of sand (white) and shale (black), (b) synthetic seismic response (same trace repeated 25 times) using a 20 Hz zero-phase Ricker wavelet, (c) frequency gather based on a CLSSA 40 ms window time-frequency analysis of a single trace from the synthetic seismic, and (d) phase gather yielded by the PD of a single trace from the synthetic seismic response.

Visually, a more appreciable change with layering might be observed on the actual location of the center of mass (CoM) or gravity of the attributes. For any discrete seismic attribute trace x within a vertical window/interval containing N samples, the location of CoM t_c of the attribute within the interval is defined as follows (Barnes, 2016):

$$t_c = \frac{\sum_{k=1}^N t_k x_k^2}{\sum_{k=1}^N x_k^2}, \quad (3)$$

where t_k is the two-way traveltime measured relative to the start of a vertical interval/window. If the interval thickness is Δt , then the attribute is said to be evenly distributed whenever $t_c = \Delta t/2$. In cases where $t_c < \Delta t/2$, its energy is mostly concentrated on the top half of the interval, whereas $t_c > \Delta t/2$ means that its energy is mostly concentrated in the bottom half. A better-known attribute that expresses the CoM or concentration of energy concept is called the energy half-time E_{ht} , which expresses the CoM location as a percentage of the interval length (Barnes, 2016):

$$E_{ht} = 100\% \cdot \left(\frac{t_c}{\Delta t} \right). \quad (4)$$

The term $E_{ht} = 50\%$ means that attribute's energy is evenly distributed within the window/interval; if $E_{ht} < 50\%$, then most of the attribute energy is said to be concentrated on the top half of the window or interval. If $E_{ht} > 50\%$, then most of the energy concentration occurs on the bottom half of the window/interval. Skewness S (McKillup and Darby, 2010; Spiegel et al., 2013) is a metric interpretable in a similar way to all of the above, but it is mostly applied to distributions, rather than directly applied to time/depth series as seismic attributes.

The main spectral attributes from time-frequency analysis such as peak magnitude and peak frequency can be extracted from the frequency gather for a corresponding modeled sequence. In addition, because models are built using a zero-phase wavelet, then individual orthogonal phase component traces can be extracted from the phase gather, such as the odd trace (-90° plus $+90^\circ$) and the even trace (0° plus 180°). We could then calculate all the metrics mentioned earlier to assess how the thin-bed layering distribution influences the symmetry of spectral-based seismic attributes. Figure 10 shows a collection of spectral attributes for a 20 ms thick 100% NTG layer, and how metrics (displayed on the top of each track) for each attribute compare with the true metric values of the stratal sequence being modeled. For the case of the CoM, it is graphically represented at a dashed line at each track. The windows used to calculate

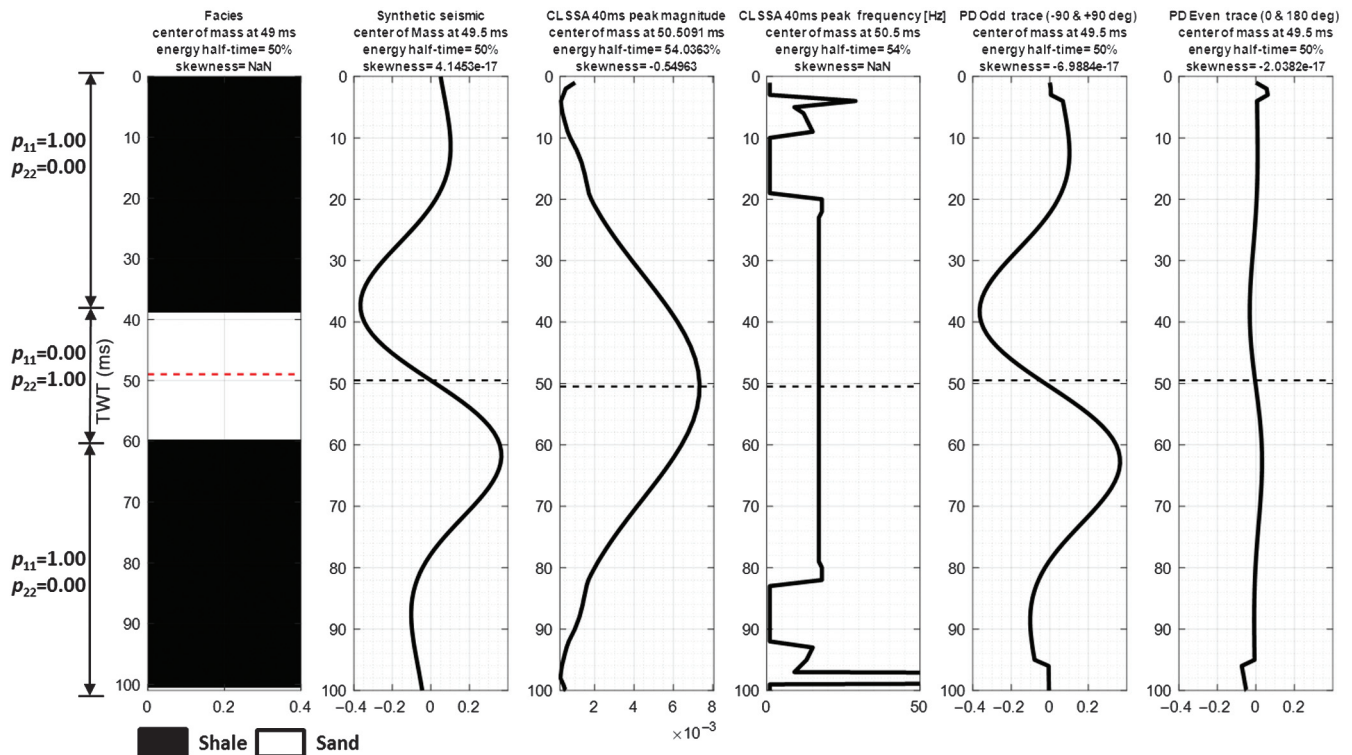


Figure 10. Simulation (base case) using the conditional probabilities indicated on the far left for a 20 ms long stratal binary sequence: (a) bed facies model displaying interbedded layers of sand (white) and shale (black), (b) synthetic seismic response using a 15 Hz zero-phase Ricker wavelet, (c) CLSSA peak magnitude, (d) CLSSA peak frequency (Hz), (e) PD odd trace (-90° and $+90^\circ$), and (f) PD even trace (0° and 180°). On the top of each track, there is the corresponding CoM location, energy half-time, and skewness. The interval for metric calculation for tracks (b-f) is defined by the interpreted top and base event on the seismic trace on (b). The CoM for each track is shown as a dashed line.

the metrics for all attributes are bounded by the top and base events associated with the layer as interpreted on the synthetic seismic. Given the homogeneity of the bed, all the metrics are in very close agreement to what would be expected of a bed with vertical symmetry of its layering. CoM differences among attributes are within the current time sampling interval ($dt = 1$ ms).

Figure 11 shows an example of Markov-based layering as described earlier, with displays similar to those in Figure 10. Based on these and all other simulations we performed during this research (but for brevity not shown in this paper), all layering symmetry metrics across attributes are in close agreement with the true metrics of the bed within the limits of time sampling, which cannot provide any robust insight about the underlying overall layering distribution within the bed. Another important observation is that PD preferential illumination is achieved for the odd trace, regardless of internal variations of the bed layering. This may be a consequence of the binary-impedance assumption made, which combined with subtuning interference causes the output seismic signal to be always preferentially illuminated by the odd component of PD.

External interference on a thin bed

Until this point, we have only shown the effects of internal binary layering on spectral attributes for a seis-

mically isolated thin bed. Variations in such internal layering are not manifested into clear distinguishable responses in seismic attributes derived from time-frequency and time-phase analysis. Introducing some internal reflectivity for the encasing media is expected to achieve a certain level of mutual interference with the target bed that may be used as an avenue to draw inferences about the underlying stratigraphy of the encasing media. Figures 12 and 13 show some simulations for a target thin bed as shown in Figure 10, but introducing external interference by embedding some binary reflectivity within the encasing media via Markov-based layering generation. This layering of the encasing media introduces different degrees of preferential phase illumination and mismatches between the CoM and other metrics measured on the attributes and the actual metrics of the target layer. Because complex interference patterns are taking place among all reflecting interfaces, a systematic effect of such patterns appears to be very elusive. However, two inferences may be made: First, there will be assemblies of reflecting events for binary sequences that would cause preferential phase illumination to be achieved on the even component instead of the odd component for a seismically thin bed. Second, the CoM of the peak frequency closely tracks that of the actual target bed in the case when external interference is present. The peak frequency CoM differ-

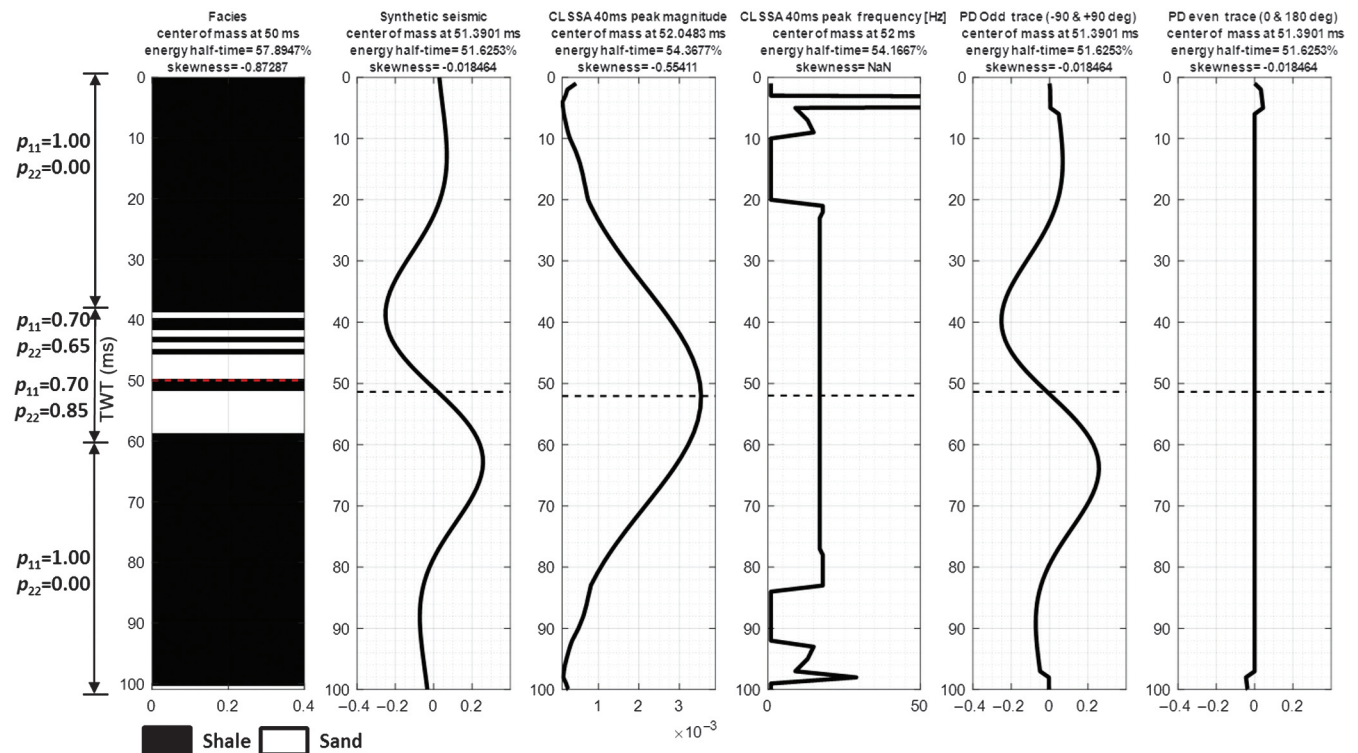


Figure 11. Simulation using the conditional probabilities indicated on the far left for a 20 ms long stratal binary sequence: (a) bed facies model displaying interbedded layers of sand (white) and shale (black), (b) synthetic seismic response using a 15 Hz zero-phase Ricker wavelet, (c) CLSSA peak magnitude, (d) CLSSA peak frequency (Hz), (e) PD odd trace (-90° and $+90^\circ$), and (f) PD even trace (0° and 180°). On the top of each track, there is the corresponding CoM location, energy half-time, and skewness. The interval for metric calculation for tracks (b-f) is defined by the interpreted top and base event on the seismic trace on (b). The CoM for each track is shown as a dashed line.

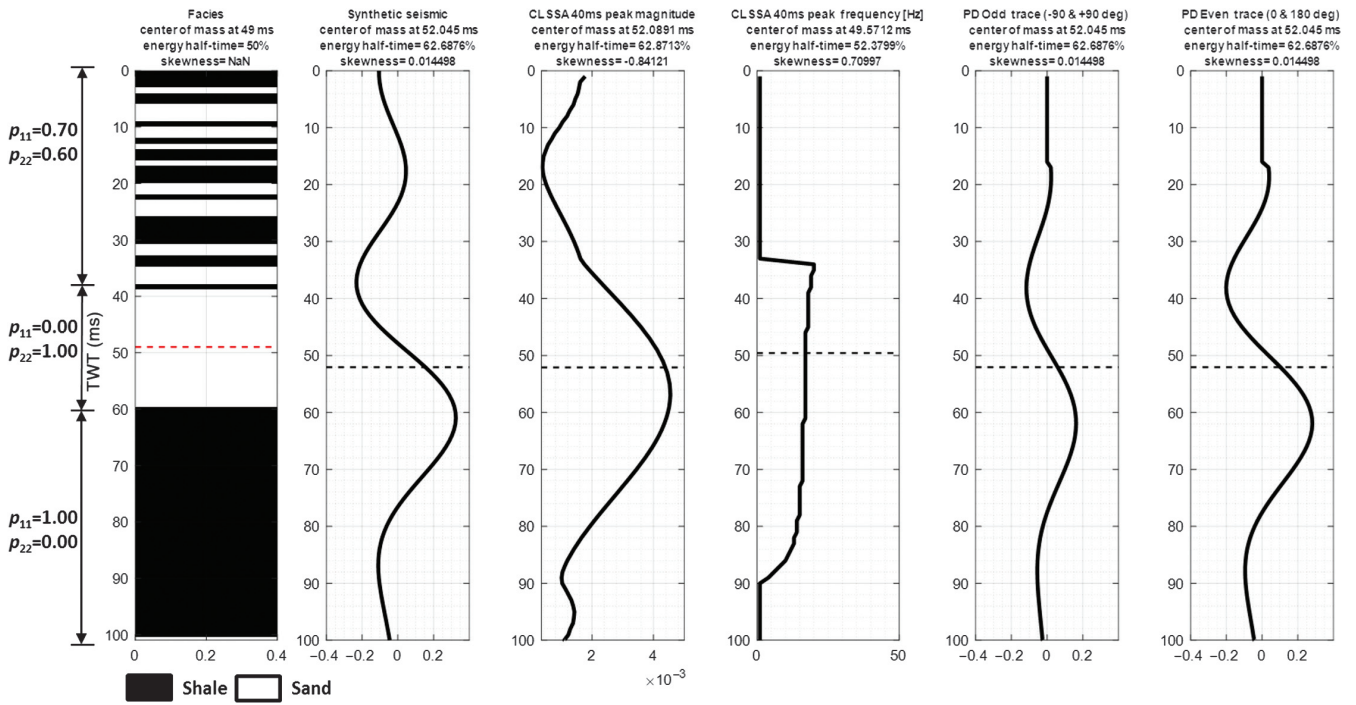


Figure 12. Simulation 1 using the conditional probabilities indicated on the far left for a 20 ms long stratal binary sequence: (a) bed facies model displaying interbedded layers of sand (white) and shale (black), (b) synthetic seismic response using a 15 Hz zero-phase Ricker wavelet, (c) CLSSA peak magnitude, (d) CLSSA peak frequency (Hz), (e) PD odd trace (-90° and $+90^\circ$), and (f) PD even trace (0° and 180°). On the top of each track, there is the corresponding CoM location, energy half-time, and skewness. The interval for metric calculation for tracks (b-f) is defined by the interpreted top and base event on the seismic trace on (b). The CoM for each track is shown as a dashed line.

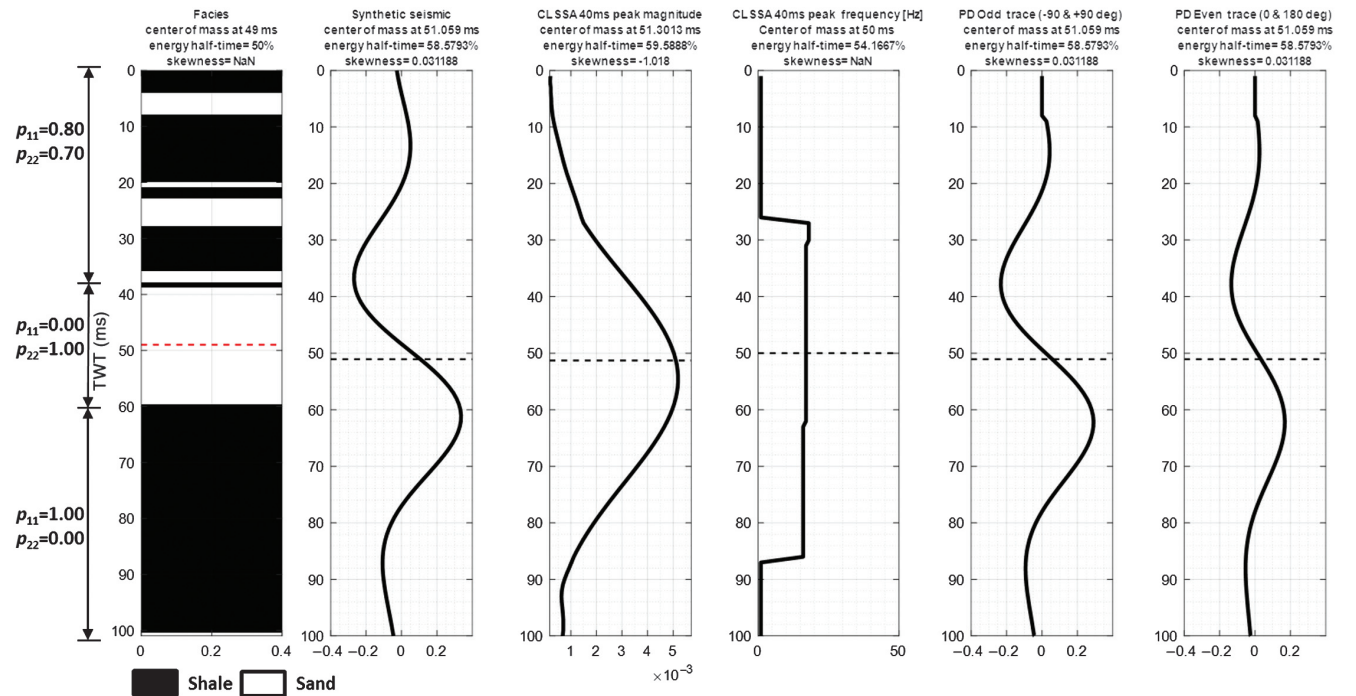


Figure 13. Simulation 2 using the conditional probabilities indicated on the far left for a 20 ms long stratal binary sequence: (a) bed facies model displaying interbedded layers of sand (white) and shale (black), (b) synthetic seismic response using a 15 Hz zero-phase Ricker wavelet, (c) CLSSA peak magnitude, (d) CLSSA peak frequency (Hz), (e) PD odd trace (-90° and $+90^\circ$), and (f) PD even trace (0° and 180°). On the top of each track, there is the corresponding CoM location, energy half-time, and skewness. The interval for metric calculation for tracks (b-f) is defined by the interpreted top and base event on the seismic trace on (b). The CoM for each track is shown as a dashed line.

ence with respect to the rest of attributes CoM might be larger than the time sampling on this noise-free scenario, therefore opening a possibility of using peak frequency to assess external layer interference.

The effect of external interference on the spectral response of a targeted thin bed can be better illustrated analytically: For a given central or peak frequency f , the time response over t of a Ricker wavelet Rw is defined as follows (Sheriff, 2002):

$$Rw(t) = (1 - 2\pi^2 f^2 t^2) e^{-\pi^2 f^2 t^2}. \quad (5)$$

For a binary impedance space, the seismic response of a thin bed can be represented by a scaled version of the first derivative of the wavelet with respect to time (Widess, 1973), which takes the following analytical form for a Ricker wavelet:

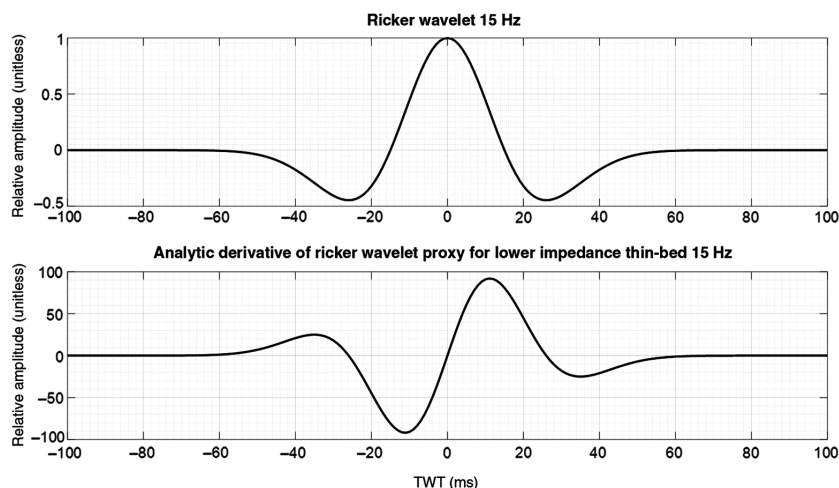


Figure 14. (a) Time response of a zero-phase 15 Hz Ricker wavelet, (b) analytic derivative of the Ricker wavelet on (a), representing a lower impedance thin-bed seismic waveform.

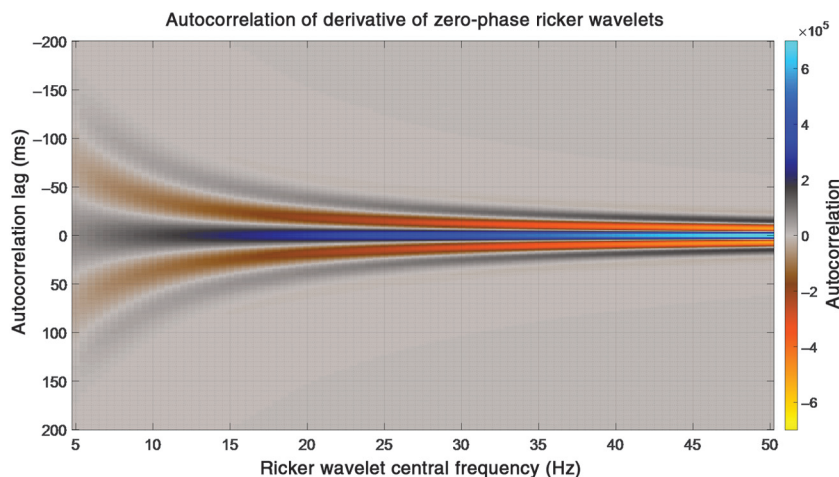


Figure 15. Crosscorrelation of two identical waveforms of thin beds, based on a scaled derivative of a zero-phase Ricker wavelet with varying central frequency.

$$\frac{\delta Rw}{\delta t} = (e^{-\pi^2 f^2 t^2})(-6\pi^2 f^2 t + 4\pi^4 f^4 t^3). \quad (6)$$

Figure 14 shows an example of a zero-phase 15 Hz Ricker wavelet time response (Figure 14a) and its corresponding derivative (Figure 14b), which represents the scaled waveform for a lower impedance thin-bed convolved with a 15 Hz zero-phase Ricker wavelet. Two thin-bed responses are expected to yield different composite seismic traces depending on the proximity of the two waveforms, which would produce differences in the time-frequency and time-phase responses. This is especially true for cases in which constructive and destructive interference are achieved, which can be estimated via the crosscorrelation of the two thin-bed waveforms, as shown in Figure 15, which depicts the crosscorrelation of two identical thin-bed waveforms

as a function of the Ricker-wavelet central frequency. Constructive interference is represented with cold colors, and the destructive interference is represented with warm colors. The lower the frequency, the larger the required vertical separation between the two thin-bed waveforms to avoid mutual interference.

Because the proximity of two thin-bed waveforms can yield different interference patterns the time-frequency and time-phase analyses are expected to respond accordingly. Figures 16–19 depict some of such responses for time lags associated with the maximum constructive and destructive interference of the derivative of a zero-phase 15 Hz Ricker wavelet, as determined from the crosscorrelation depicted in Figure 15. The time-frequency and time-phase analyses correspond to those of the composite signal resulting from the summation of the two thin-bed waveforms for a given time lag. Figure 16 shows the case in which the interfering thin bed (most of it is outside the TWT range) is so far of the reference thin bed that the two thin beds are nearly seismically isolated; therefore, the interference effects are not manifested on the frequency and phase gathers, with the latter achieving preferential phase illumination approximately -90° for the reference thin bed (whose center is located approximately 100 ms), as expected.

For cases in which the time lag between waveforms is such that maximum destructive interference is achieved (it is subtle in Figure 17 and more pronounced in Figure 19), then the preferential phase illumination is achieved at phase components significantly differ-

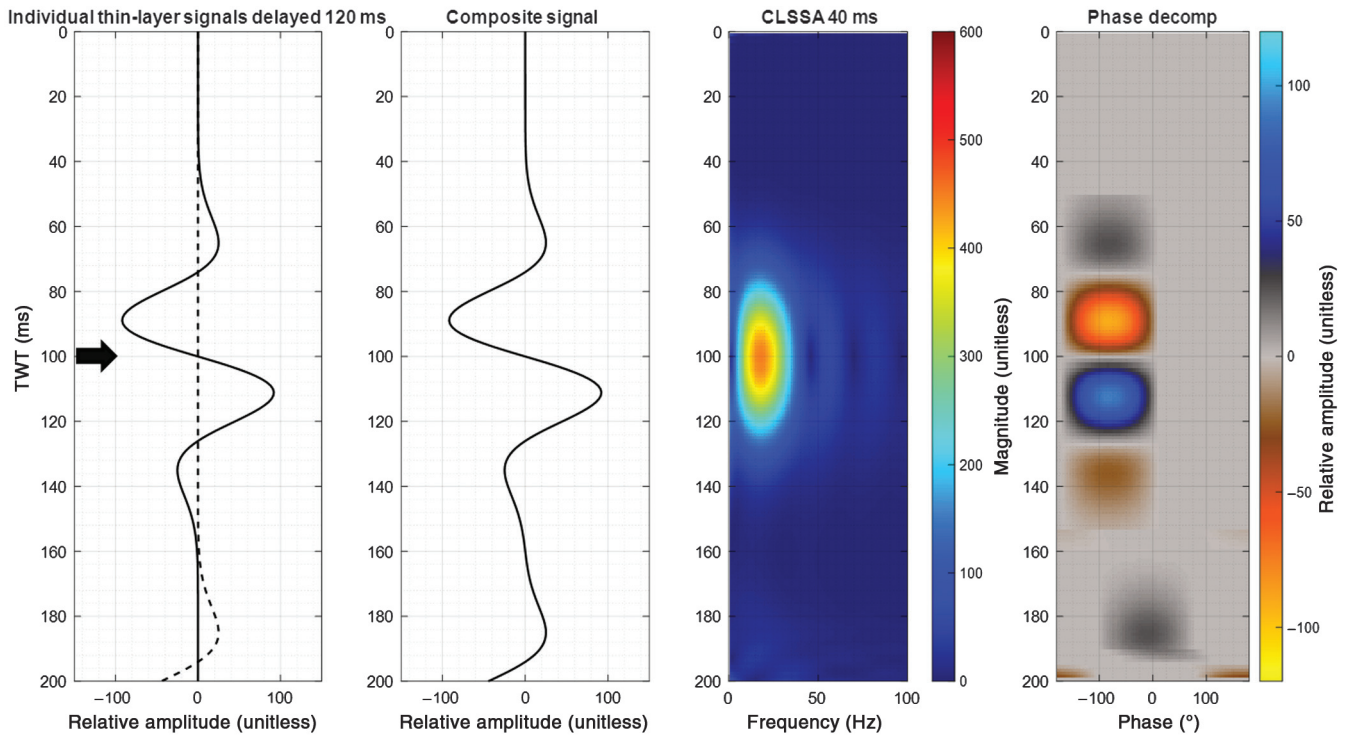


Figure 16. Time-variant spectral responses of the combination of two mutually interfering thin-bed waveforms with their centers (highlighted with arrows) separated 120 ms: (a) reference (targeted) thin-bed waveform (the solid line) and interfering thin-bed waveform (the dashed line), (b) composite (summation of the two thin-bed waveforms) seismic response of the waveforms shown in (a), (c) CLSSA time-frequency analysis of the composite seismic response, and (d) PD time-phase analysis of the composite seismic response.

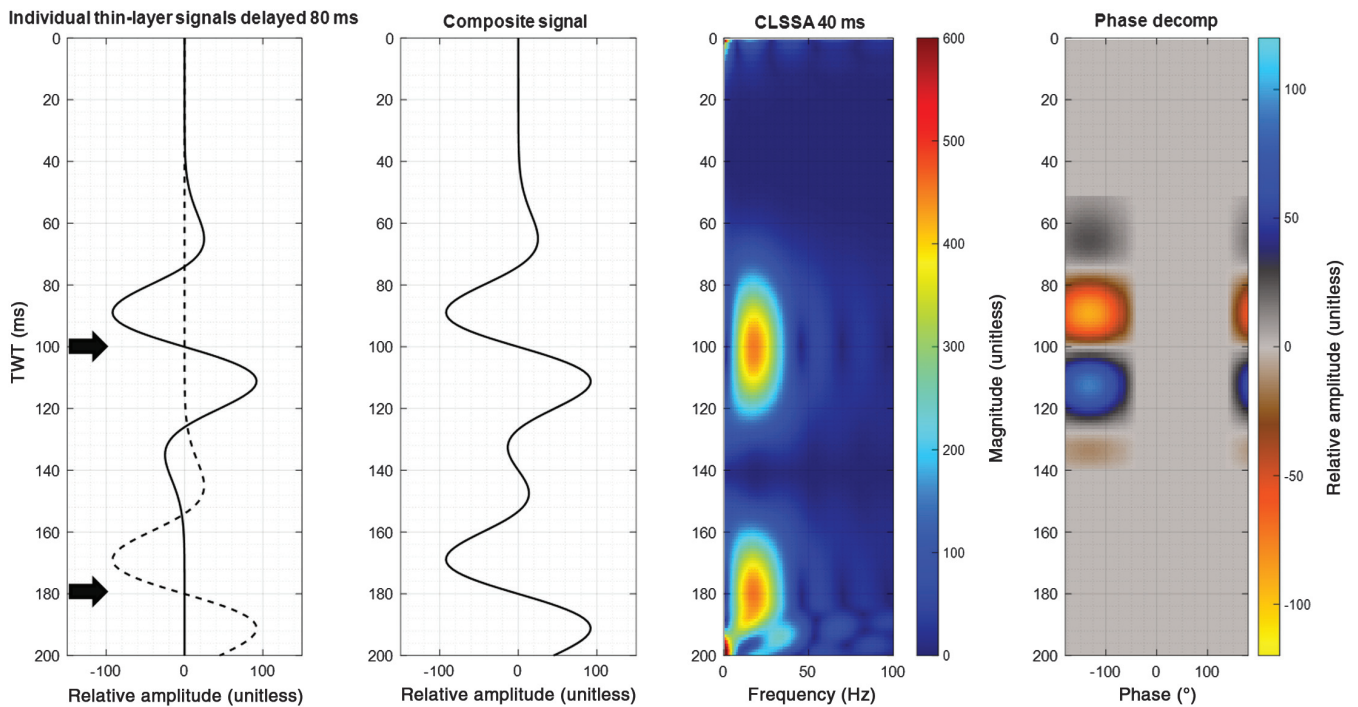


Figure 17. Time-variant spectral responses of the combination of two mutually interfering thin-bed waveforms with their centers (highlighted with arrows) separated 80 ms: (a) reference (targeted) thin-bed waveform (the solid line) and interfering thin-bed waveform (the dashed line), (b) composite (summation of the two thin-bed waveforms) seismic response of the waveforms shown in (a), (c) CLSSA time-frequency analysis of the composite seismic response, and (d) PD time-phase analysis of the composite seismic response.

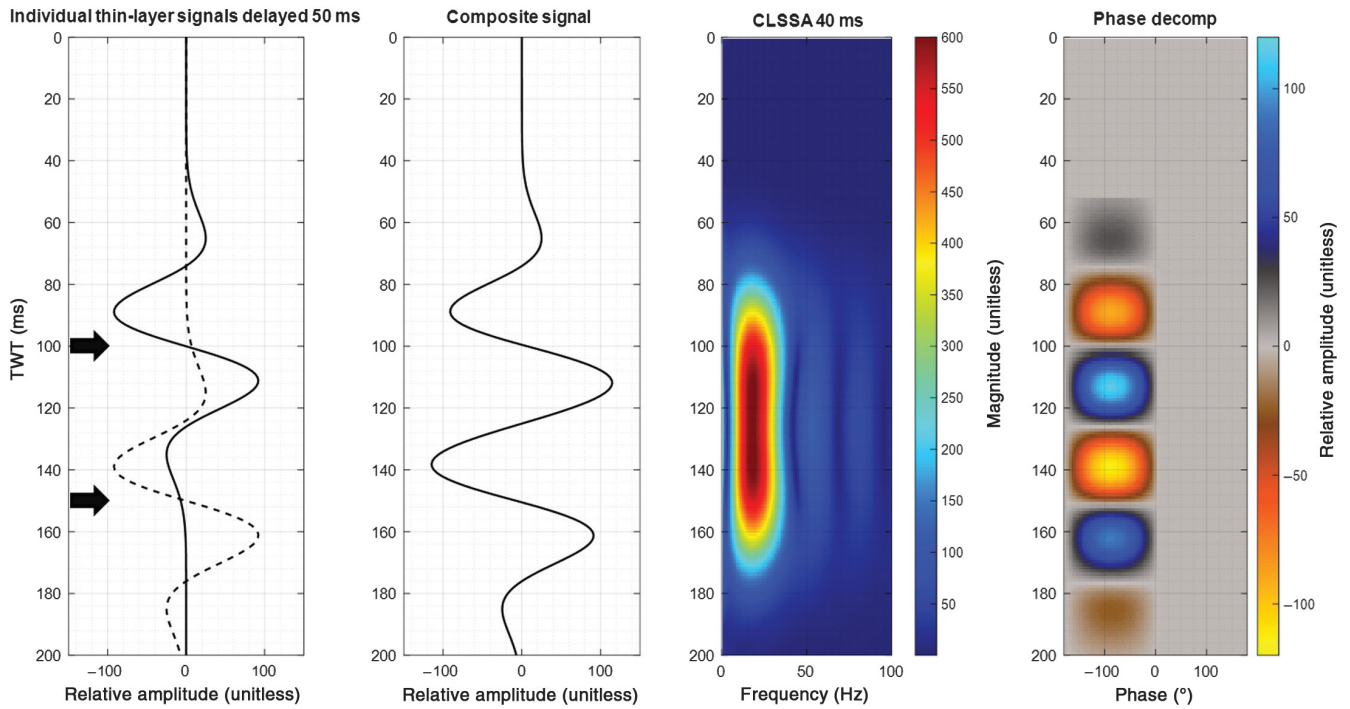


Figure 18. Time-variant spectral responses of the combination of two mutually interfering thin-bed waveforms with their centers (highlighted with arrows) separated 50 ms: (a) reference (targeted) thin-bed waveform (the solid line) and interfering thin-bed waveform (the dashed line), (b) composite (summation of the two thin-bed waveforms) seismic response of the waveforms shown in (a), (c) CLSSA time-frequency analysis of the composite seismic response, and (d) PD time-phase analysis of the composite seismic response.

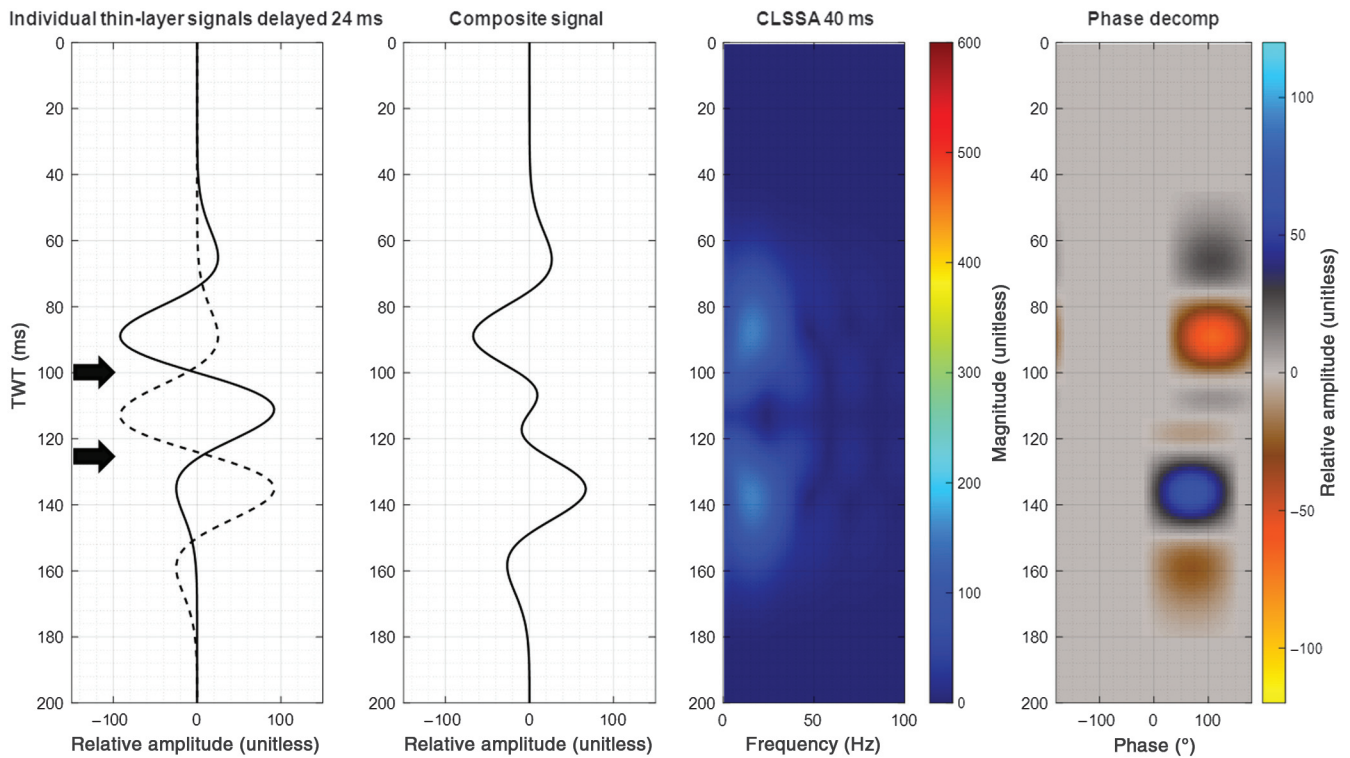


Figure 19. Time-variant spectral responses of the combination of two mutually interfering thin-bed waveforms with their centers (highlighted with arrows) separated 24 ms: (a) reference (targeted) thin-bed waveform (the solid line) and interfering thin-bed waveform (the dashed line), (b) composite (summation of the two thin-bed waveforms) seismic response of the waveforms shown in (a), (c) CLSSA time-frequency analysis of the composite seismic response, and (d) PD time-phase analysis of the composite seismic response.

ent than -90° , whereas the preferential frequency illumination remains essentially unchanged, despite the large reduction of the peak amplitude. Figure 18 represents the case for a time lag in which maximum constructive interference is achieved (for a nonzero lag): The preferential phase illumination is close to -90° for the reference thin bed, whereas the preferential frequency illumination remains unchanged, despite the expected increase of the peak magnitude.

The phase component that yields preferential phase illumination is then dependent on the proximity of the mutually interfering thin-bed waveforms and also on the underlying wavelet. A compact, short-lived time response (or coda) of the wavelet, also characterized by few low-amplitude sidelobes, would be more limited in its reach to cause mutual interference with neighboring thin beds. These desired wavelet characteristics can only be achieved by obtaining seismic data with the broadest bandwidth and as close to zero phase as possible, leading to the improvement of the seismic isolation of thin beds being targeted.

Conclusion

The seismic forward modeling of a seismically isolated thin bed with uniformly distributed interbedded binary impedance layers (sands and shales) shows that the composite amplitude of the bed increases with NTG, behavior that is very similar to that exhibited by time-frequency analysis' peak magnitude, whereas the peak frequency does not show any correlation with varying NTG, as shown in Figure 2. The time-phase analysis' peak amplitude variation with varying NTG is very close to that of the composite amplitude mentioned above, whereas the phase component that preferentially illuminates the thin bed (i.e., the peak phase on the time-phase analysis) remains unchanged regardless of the underlying NTG, as shown in Figure 5. In the case in which more complex (nonuniformly distributed) layering is modeled via Markov chains, then the magnitude of the peak amplitude of the time-frequency and time-phase analysis for a thin-bed increases with the NTG, whereas the frequency and phase components that preferentially illuminate the bed on each simulation remain essentially constant. All of these observations lead us to conclude that, for an isolated thin-bed composed of interbedded binary impedance layers, the NTG signature is observed on the amplitude (magnitude) responses, rather than any specific frequency or phase component.

When considering a target thin bed with 100% NTG, we introduced layers on the background (shale) media using also a Markov-chain-layering generation process, to create seismic interference on the target bed seismic response. Even though the time-frequency analysis' peak magnitude and peak frequency at the target respond to different interfering layering, the time-phase analyses' phase component that preferentially illuminates the target bed changes — although not systematically — with different interfering layering simulations.

In the case that the embedded seismic wavelet is known, for an isolated thin-bed encased on a homogeneous media, the target bed seismic response can be modeled as a scaled version of the derivative of the wavelet. The autocorrelation of the derivative of the wavelet can provide the nonzero vertical separation between the centers of two (elastically similar) thin beds in which mutually constructive and destructive interference occur. Therefore, this autocorrelation function represents an appropriate tool for proximity analysis of mutually interfering thin beds. While performing the time-phase analysis of the target bed, if another thin bed with comparable elastic properties is at a vertical distance such that mutual constructive interference occurs, then the phase component that would preferentially illuminate the target bed will be very close to the same phase component that preferentially illuminates the target bed when this is seismically isolated (-90° if the zero-phase embedded wavelet and target bed is lower impedance compared with the encasing background media). Mutually destructive interference will dramatically change the phase preferential illumination of the target bed away from that of a seismically isolated case.

Acknowledgments

The authors wish to thank J. Mauricio Florez, C. Moreno, M. Silva, O. Portniaguine, Lumina Geophysical, and The University of Houston. Our thanks go to BHP for its support.

Data and materials availability

Data associated with this research are confidential and cannot be released.

References

- Avseth, P., T. Mukerji, and G. Mavko, 2010, Quantitative seismic interpretation: Applying rock physics tools to reduce interpretation risk: Cambridge University Press.
- Bailey, R. J., and D. G. Smith, 2005, Quantitative evidence for the fractal nature of the stratigraphic record: Results and implications: Proceedings of the Geologists' Association, **116**, 129–138, doi: [10.1016/S0016-7878\(05\)80004-5](https://doi.org/10.1016/S0016-7878(05)80004-5).
- Barnes, A. E., 2016, Handbook of poststack seismic attributes: SEG, Geophysical References Series 21.
- Bracewell, R. N., 2000, The Fourier transform and its applications: McGraw-Hill.
- Browaeyes, T. J., and S. Fomel, 2009, Fractal heterogeneities in sonic logs and low-frequency scattering attenuation: Geophysics, **74**, no. 2, WA77–WA92, doi: [10.1190/1.3062859](https://doi.org/10.1190/1.3062859).
- Brown, A. R., R. M. Wright, K. D. Burkart, and W. L. Abriel, 1984, Interactive seismic mapping of net producible gas sand in the Gulf of Mexico: Geophysics, **49**, 686–714, doi: [10.1190/1.1441698](https://doi.org/10.1190/1.1441698).
- Brown, A. R., R. M. Wright, K. D. Burkart, W. L. Abriel, and R. G. McBeath, 1986, Tuning effects, lithological effects and depositional effects in the seismic response of gas

reservoirs: *Geophysical Prospecting*, **34**, 623–647, doi: [10.1111/j.1365-2478.1986.tb00485.x](https://doi.org/10.1111/j.1365-2478.1986.tb00485.x).

Castagna, J. P., A. Oyem, O. N. Portniaguine, and U. Aikulola, 2016, Phase decomposition: Interpretation, **4**, no. 3, SN1–SN10, doi: [10.1190/INT-2015-0150.1](https://doi.org/10.1190/INT-2015-0150.1).

Castagna, J. P., S. Sun, and R. W. Siegfried, 2003, Instantaneous spectral analysis: Detection of low-frequency shadows associated with hydrocarbons: *The Leading Edge*, **22**, 120–127, doi: [10.1190/1.1559038](https://doi.org/10.1190/1.1559038).

Chakraborty, A., and D. Okaya, 1995, Frequency-time decomposition of seismic data using wavelet-based methods: *Geophysics*, **60**, 1906–1916, doi: [10.1190/1.1443922](https://doi.org/10.1190/1.1443922).

Chopra, S., and J. P. Castagna, 2014, AVO: SEG, *Investigations in Geophysics* 16.

Connolly, P. A., 2007, A simple, robust algorithm for seismic net pay estimation: *The Leading Edge*, **26**, 1278–1282, doi: [10.1190/1.2794386](https://doi.org/10.1190/1.2794386).

Davis, J. C., 2002, *Statistics and data analysis in geology*: Wiley.

Dimri, V. P., 2005, *Fractal behavior of the earth system*: Springer.

Dolan, S. S., C. J. Bean, and B. Rioulet, 1998, The broadband fractal nature of heterogeneity in the upper crust from petrophysical logs: *Geophysical Journal*, **132**, 489–507, doi: [10.1046/j.1365-246X.1998.00410.x](https://doi.org/10.1046/j.1365-246X.1998.00410.x).

Dvorkin, J., M. A. Gutierrez, and D. Grana, 2014, *Seismic reflections of rock properties*: Cambridge University Press.

Lancaster, S., and D. Whitcombe, 2000, Fast-track ‘colored’ inversion: 70th Annual International Meeting, SEG, Expanded Abstracts, 1572–1575.

McKillup, S., and M. Darby, 2010, *Geostatistics explained: An introductory guide for earth scientists*: Cambridge University Press.

Meza, R. G., G. Haughey, J. P. Castagna, U. Barbato, and O. N. Portniaguine, 2016, Phase decomposition as a hydrocarbon indicator: a case study: 86th Annual International Meeting, SEG, Expanded Abstracts, 1839–1843.

Miall, A. D., 2010, *The geology of stratigraphic sequences*: Springer.

Okaya, D. A., 1995, Spectral properties of the earth’s contribution to seismic resolution: *Geophysics*, **60**, 241–251, doi: [10.1190/1.1443752](https://doi.org/10.1190/1.1443752).

Partyka, G., J. Gridley, and J. Lopez, 1999, Interpretational applications of spectral decomposition in reservoir characterization: *The Leading Edge*, **18**, 353–360, doi: [10.1190/1.1438295](https://doi.org/10.1190/1.1438295).

Puryear, C. I., and J. P. Castagna, 2008, Layer-thickness determination and stratigraphic interpretation using spectral inversion: Theory and application: *Geophysics*, **73**, no. 2, R37–R48, doi: [10.1190/1.2838274](https://doi.org/10.1190/1.2838274).

Puryear, C. I., O. N. Portniaguine, C. M. Cobos, and J. P. Castagna, 2012, Constrained least-squares spectral analysis: Application to seismic data: *Geophysics*, **77**, no. 5, V143–V167, doi: [10.1190/geo2011-02](https://doi.org/10.1190/geo2011-02).

Sheriff, R. E., 2002, *Encyclopedic dictionary of exploration geophysics*: SEG.

Simm, R., and M. Bacon, 2014, *Seismic amplitude: An interpreter’s handbook*: Cambridge University Press.

Spiegel, M. R., J. Schiller, and R. A. Srinivasan, 2013, *Probability and statistics*: McGraw-Hill.

Turcotte, D. L., 1997, *Fractals and chaos in geology and geophysics*: Cambridge University Press.

Widess, M. B., 1973, How thin is a thin bed?: *Geophysics*, **38**, 1176–1180, doi: [10.1190/1.1440403](https://doi.org/10.1190/1.1440403).



Ramses Meza received an M.S. in geophysics from the Colorado School of Mines (USA) and geophysical engineering degree from the Universidad Simon Bolivar (Venezuela) and a Ph.D. in geophysics from the University of Houston. He is a principal geophysicist with BHP Petroleum. Early in his career he worked as a reservoir geophysicist at PDVSA in Puerto La Cruz, Venezuela; Harvest-Vinccler in Maturin, Venezuela; and ConocoPhillips in Houston, USA. His responsibilities included support in terms of quantitative seismic interpretation for hydrocarbon exploration and production activities. Since 2012, he has been with BHP as a subject-matter expert providing advanced geophysical support to all E&P assets with emphasis on integration of QI products, visualization, seismic attributes, QI quality assurance, seismic reservoir characterization, direct hydrocarbon indicator (DHI) analysis, and risking. He is a member of SEG, AAPG, EAGE, and SOVG.



J. Antonio Sierra received a B.S. in geology and geophysics and an M.S. in geophysics from the University of Houston. Currently, he is an exploration geophysicist at EOG Resources focused on generating prospects in the Columbus Basin, offshore Trinidad and Tobago. In addition, he has designed and executed seismic acquisition and processing campaigns optimized for detailed structural and quantitative seismic interpretation. He was previously a geophysicist at BHP Billiton as part of their rock and fluid physics team doing quantitative seismic interpretation for conventional and unconventional plays. While at BHP Billiton, he also worked in the seismic processing and imaging team with a focus on building seismic velocity models.



John P. Castagna received a B.S. (1976) in geology from Brooklyn College and an M.S. (1981) in high-temperature geochemistry. He completed his doctoral degree in exploration geophysics from the University of Texas at Austin in 1983. He specializes in exploration geophysics research and development. He is widely known for his

work in direct hydrocarbon detection and reservoir characterization. He joined ARCO's well-logging research group in 1980. He served the company in several research, exploration, field development, and management positions. In 1982, he was named technical coordinator for Sonic Logging Research; in 1986, log analyst for Reservoir Engineering Services; in 1987, technical coordinator for Rock Physics Research; in 1988, director of Geoseismic Interpretation Research; and in 1989, manager of Seismic Analysis Research. In 1990, he transferred to Vastar Resources where he was responsible for the development of an extension of major offshore Gulf of Mexico fields and exploration of surrounding acreage. He later joined ARCO International Oil and Gas Co., with the responsibility of offshore China and Russia exploration. He returned to ARCO Research in 1995 and was assigned as visiting research scientist at the Geotechnology Research Institute of the Houston Advanced Research Center, where he was principal investigator for research projects funded by the Gas Research Institute, the Energy Research Clearing House, and a consortium of energy companies. Also in 1995, he was named distinguished lecturer for SEG, delivering the fall lecture on "Applied AVO analysis: Use and abuse of amplitude variation with offset." He has served SEG in various other capacities including as chairman of *The Leading Edge* editorial board, first vice-

president, and technical program chairman for the 2003 Annual Convention in Dallas. His book, *Offset-Dependent-Reflectivity: Theory and Practice of AVO Analysis*, is an SEG bestseller. He has also served as associate editor for GEOPHYSICS. In 2000, he founded Fusion Geophysical, a geophysical contractor specializing in integrated seismic analysis. In February 2010, he founded Lumina Geophysical, leading the industry in seismic spectral analysis, QI, and reservoir characterization. He currently holds the Robert Sheriff Chair of Geophysics at the University of Houston. His main technical interest is quantitative seismic analysis in exploration and reservoir characterization.



Umberto Barbato received an M.S. in geophysics and seismology from the University of Houston. He is the manager of Case Studies at Lumina Geophysical; he has more than five years of experience working in the oil and energy industry. He is skilled in seismic interpretation, geophysics, earth science, and petroleum geology and has several publications in spectrally based seismic attributes.